Critical-Current Memory of In-Plane Superconducting Domains in Kagome RbV_3Sb_5

Sheng-Biao Sun(孙圣彪),[1,*] Jia-Peng Peng(彭家鹏),[1,*] Qian-Hui Sun(孙千惠),[1,*] Liang Xiong(熊亮),[1] Lang Xiao(肖朗),[1] Jing-Quan Li(李京权),[1] Jian-Kun Wang(王建坤),[1] Ben-Chuan Lin(林本川),[2,†] and Shuo Wang(王硕)[2,‡]

[1] *Shenzhen Institute for Quantum Science and Engineering, Southern University of Science and Technology, Shenzhen 518055, China*
[2] *International Quantum Academy, and Shenzhen Branch, Hefei National Laboratory, Shenzhen,518048, China.*

(Dated: August 9, 2026)

The kagome superconductors AV_3Sb_5 ($A = \mathrm{K, Rb, Cs}$) host charge order, nematicity, and superconductivity, but the specific superconducting pairing mechanism remains unclear. Here we report critical-current memory in exfoliated RbV_3Sb_5 under in-plane magnetic fields. Magnetoresistance exhibits an unconventional hysteresis, while the critical-current maximum shifts away from zero field with a sign selected by the sweep direction, appearing near -0.2 T and $+0.2$ T for opposite sweeps. On a single sweep branch, $I_c(+B) \neq I_c(-B)$, indicating the time reversal symmetry is broken. The zero-field-cooling state carries the largest current, $I_c^{\mathrm{ZFC}}(0) \simeq 35\ \mu$A, exceeding all field-trained values. The effect is absent in CsV_3Sb_5 and $NbSe_2$ controls. These results point to time-reversal symmetry breaking and trainable in-plane superconducting moments of the superconducting states in RbV_3Sb_5.

Keywords: kagome superconductor, critical-current memory, time-reversal symmetry breaking, superconducting domains
PACS: 74.25.Sv, 74.20.Rp, 74.78.-w, 74.25.F-

Introduction.—Kagome metals have emerged as an promising platform for studying correlated quantum matter because their lattice geometry can combine van Hove singularities, Dirac dispersions, flat-band tendencies, and strong geometric frustration. The superconducting family AV_3Sb_5 ($A = \mathrm{K, Rb, Cs}$) is especially important: superconductivity develops from a normal state already shaped by charge-density-wave order, rotational-symmetry breaking, possible loop-current order, and pair-density-wave modulations [1–9]. This coexistence raises a central question: is the superconducting condensate a conventional descendant of the same electronic structure in all three compounds, or does each member of the family realize a distinct pairing state?

Existing experiments suggest the second possibility. Several measurements on CsV_3Sb_5 are consistent with nodeless or sign-preserving superconductivity [10–13], whereas μSR and other probes on Rb/K compounds point to a more fragile and likely nodal superconducting state [14, 15]. At the same time, time-reversal symmetry can already be broken in the charge-ordered normal state such as loop-current physics [16–20]. Therefore an experimental signature of superconducting time-reversal-symmetry breaking must be separated from normal-state magnetism and from conventional flux trapping in mesoscopic devices.

Recent magnetotransport work on thin-flake RbV_3Sb_5 reported an in-plane-field hysteresis and a field-driven re-entrant superconducting regime [21]. A theoretical analysis proposed that these effects can arise from spin-polarized, nonunitary superconducting domains [22]. The present Letter focuses on another important stringent nonlinear observable: the critical current. Unlike a low-bias resistance, I_c measures the largest percolating supercurrent supported by the complete superconducting network. It is therefore sensitive not only to the local superconducting amplitude, but also to domain walls, weak links, and metastable textures.

In this work, we report history-dependent critical-current and magnetoresistance responses in exfoliated RbV_3Sb_5 under in-plane magnetic fields. By combining zero-field-cooling measurements, controlled field-training protocols, current-biased V-I curves, differential-resistance mapping, and comparative devices based on CsV_3Sb_5 and $NbSe_2$, we show that the superconducting state of RbV_3Sb_5 retains a memory of the field-sweep direction that is absent in the control materials. The field-trained critical-current maximum is displaced from zero field and reverses sign with sweep direction, whereas the zero-field-cooling state carries a larger global supercurrent than any field-trained state. This combination indicates a trainable internal in-plane superconducting degree of freedom: the magnetic field can bias the domain configuration, but finite-field depairing and domain-wall weak links reduce the percolating critical current. Our work further reveals the time-reversal symmetry breaking stemming from the superconducting state itself in RbV_3Sb_5 and also the special superconducting properties of RbV_3Sb_5 compared to the CsV_3Sb_5 belonging to the same family.

Experimental methods.—Thin flakes of RbV_3Sb_5, CsV_3Sb_5, and $NbSe_2$ were mechanically exfoliated from bulk crystals using polydimethylsiloxane stamps and transferred onto Si/SiO_2 substrates with pre-patterned electrodes. Electrical contacts were defined by electron-beam lithography followed by electron-beam evapora-

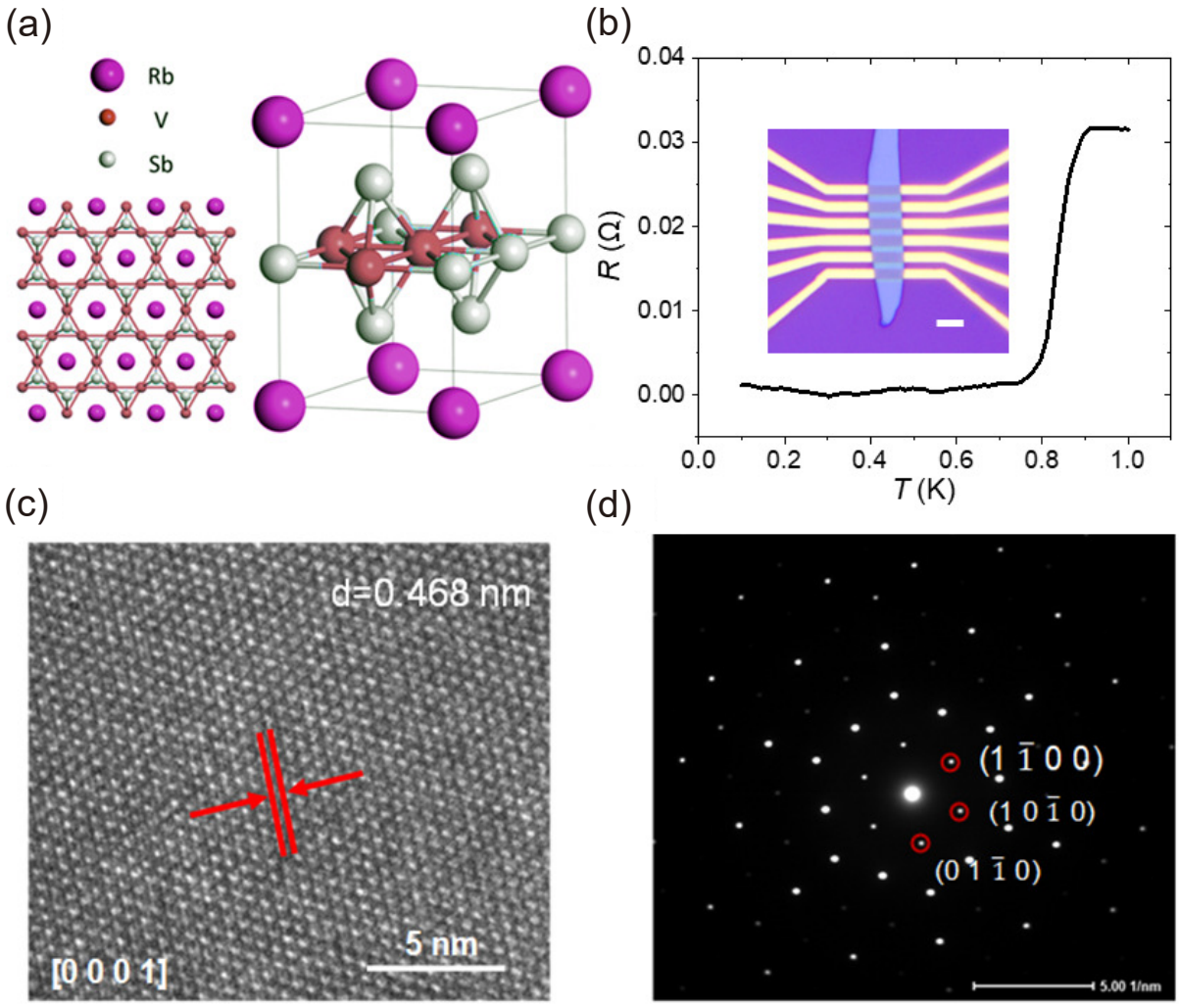


FIG. 1. **Device and crystallographic characterization of RbV_3Sb_5.** (a) Layered crystal structure of RbV_3Sb_5, with V-Sb kagome slabs separated by Rb layers. (b) Four-terminal resistance versus temperature of the thin-flake device. The superconducting transition occurs near $T_c \simeq 0.85$ K using the 50% normal-resistance criterion. The inset shows an optical micrograph of the contacted flake; the scale bar is 3 μm. (c) High-resolution transmission-electron-microscopy image showing a lattice spacing $d \simeq 0.468$ nm. (d) Selected-area electron-diffraction pattern confirming crystalline quality and crystal direction.

tion of Ti/Au electrodes with nominal thicknesses of 10/50 nm. After contacting, the devices were capped with hexagonal boron nitride to suppress degradation during air exposure. Fabrication and transfer steps were performed in an inert glovebox with oxygen and water levels below 0.01 ppm whenever possible.

Transport measurements were carried out in an Oxford Triton XL1000 dilution refrigerator and in a Physical Property Measurement System. Current-biased V-I curves were measured using a Yokogawa GS200 source meter and a Keithley 2182A nanovoltmeter. The magneto-resistance used a standard low-frequency lock-in technique with a Stanford SR830 and low-temperature filtering to reduce electrical noise and unintentional heating. For in-plane-field measurements, the vector magnets were calibrated to minimize the out-of-plane component, because even a small perpendicular component produces vortices and can obscure the intrinsic in-plane response of a quasi-two-dimensional superconductor.

Sample characterization.—The structure and basic superconducting transition of the representative RbV_3Sb_5 device are summarized in Fig. 1. Fig. 1a shows the layered crystal structure, in which V-Sb kagome slabs are separated by Rb layers. Fig. 1b shows that the resistance drops below 0.9 K, giving $T_c \simeq 0.85$ K by the 50% normal-resistance criterion. The optical image in the inset shows a multi-terminal thin-flake geometry suitable for current-biased switching measurements. The high-resolution tunneling electron microscopy (HRTEM) image in Fig. 1c and the selected-area electron-diffraction

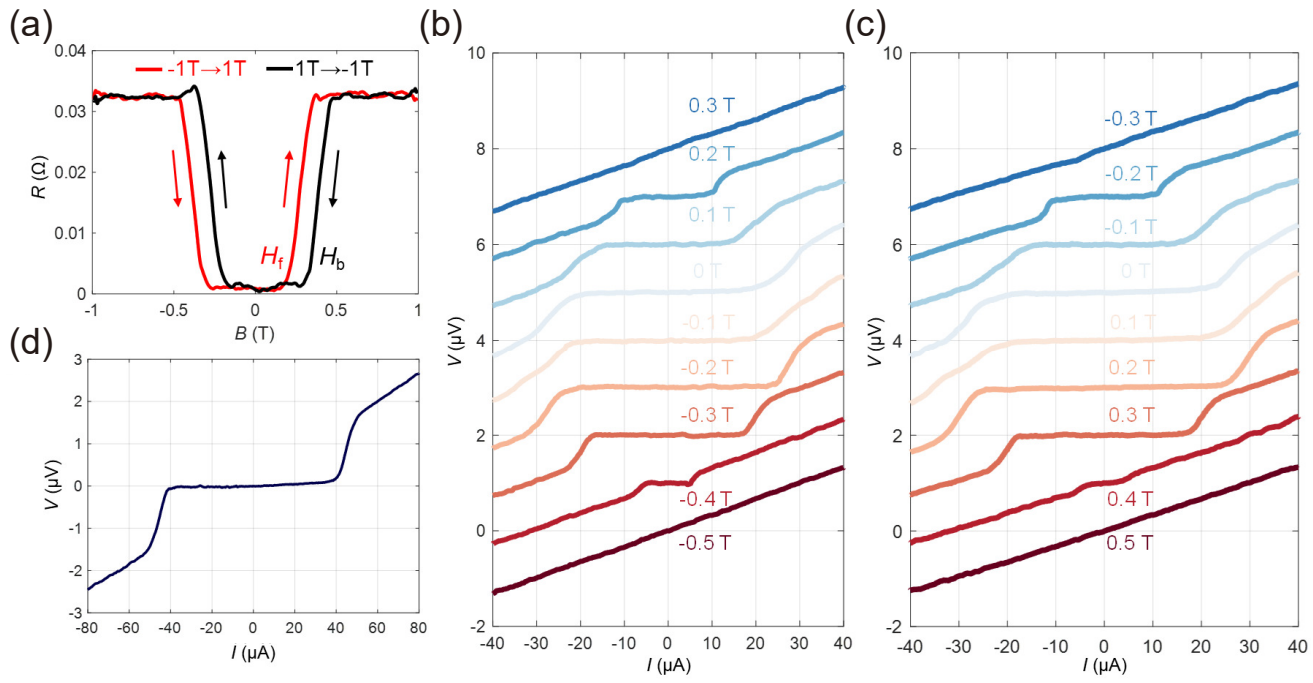


FIG. 2. **History-dependent magnetoresistance and critical current in RbV_3Sb_5.** (a) In-plane magnetoresistance measured for opposite field-sweep directions. On the positive-field side, the forward critical field H_f is smaller than the backward critical field H_b. (b) Offset V-I curves acquired during a forward in-plane-field sweep from −0.5 T to +0.3 T. The largest field-trained switching current occurs near −0.2 T. (c) Offset V-I curves acquired during a backward sweep from +0.5 T to −0.3 T. The maximum shifts to approximately +0.2 T, mirroring the forward sweep. (d) Zero-field-cooled V-I curve at $B = 0$, showing $I_c^{\mathrm{ZFC}}(0) \simeq 35$ μA, larger than the maximal field-trained value of about 25 μA in panels (b) and (c). All measurements were performed at 150 mK.

(SAED) pattern in Fig. 1d confirm that the exfoliated device preserves high crystalline quality. These characterization data are important because the hysteretic critical current discussed below cannot be attributed to a visibly granular or poorly crystalline sample.

Magnetoresistance and critical-current memory.— Fig. 2a displays the in-plane magnetoresistance hysteresis of RbV_3Sb_5. Starting from negative field and sweeping to positive field, the superconducting state survives only up to a smaller positive critical field than it does when the field is swept backward from positive to negative field. In the notation of the figure, $H_f < H_b$. This sign is opposite to the standard hysteresis of a conventional superconducting film, where superheating and supercooling typically give the reverse inequality [23–25]. It also differs from ordinary granular flux-trapping magnetoresistance, where trapped vortices or weak links produce a different return-field structure [26–29]. The same unconventional sign and metastability were reported in the previous RbV_3Sb_5 magnetotransport study [21].

The central result of this work is that the nonlinear critical current has the same memory. Fig. 2b shows V-I curves taken while sweeping the in-plane field from −0.5 T toward +0.3 T. The curves have been vertically offset for clarity. The switching current is not largest at zero field; instead, the largest field-trained value occurs near −0.2 T. Fig. 2c repeats the measurement for the opposite sweep direction, from +0.5 T toward −0.3 T. The maximum now appears near +0.2 T. Thus the preferred field is not a fixed laboratory offset, but a history-dependent quantity selected by the prior field sweep.

Fig. 2d highlights a second important observation. After zero-field cooling, the switching current at $B = 0$ is approximately 35 μA. This is substantially larger than the maximum value reached in the field-trained data, about 25 μA. At first sight this may appear puzzling: if a finite field stabilizes a trained superconducting domain, why does it not produce a larger critical current? The resolution is that the field couples to the internal superconducting moment and shifts the most favorable switching condition, but it also suppresses the supercurrent through finite-field depairing and through weak links created by metastable domain walls. This distinction between local domain energetics and global current percolation is developed qualitatively below.

The differential-resistance maps in Fig. 3 provide an independent visualization of the switching process. In the forward sweep, Fig. 3a shows that the switching features move to larger current near −0.2 T. In the backward sweep, Fig. 3b shows that the same pattern is reflected

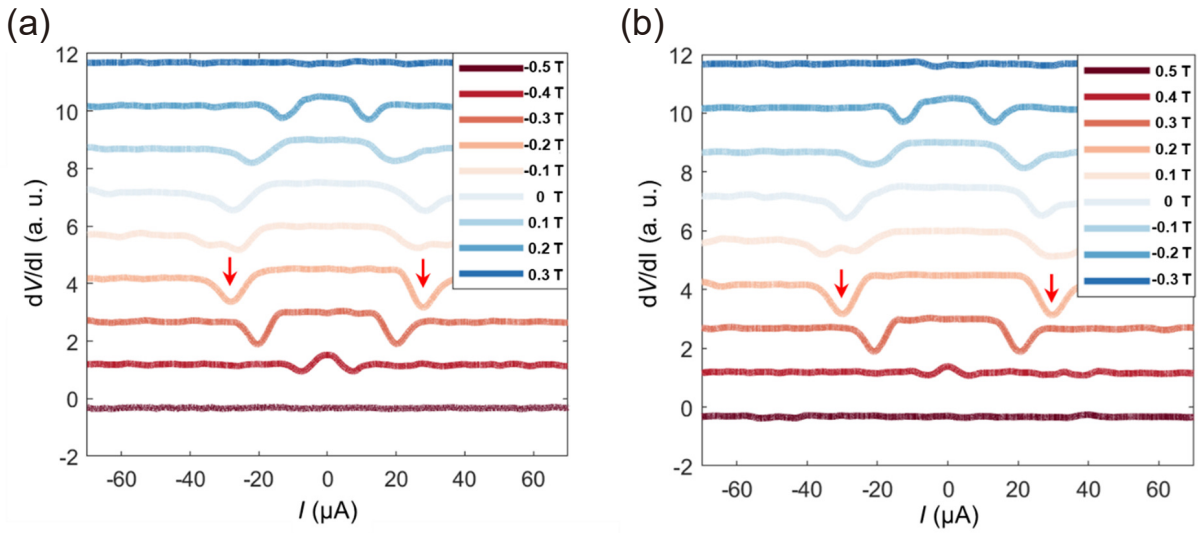


FIG. 3. **Differential-resistance representation of the switching-current memory.** (a) Differential resistance dV/dI extracted from the forward field-sweep data. The switching features evolve asymmetrically with field and reach the largest current near -0.2 T. (b) Differential resistance for the backward sweep. The pattern mirrors panel (a), with the largest switching current near $+0.2$ T. Arrows mark representative switching features. All data were obtained at 150 mK.

to the opposite field polarity. The agreement between the V-I curves and the dV/dI maps rules out an analysis artifact associated with the voltage threshold used to define I_c. Furthermore, we successfully reproduced this magnetoresistance and critical-current memory in another RbV_3Sb_5 device, confirming its intrinsic nature (Fig. S1 in Supplementary Information).

Control devices.—The control experiments in Fig. 4 are essential for excluding trivial origins. In CsV_3Sb_5, which belongs to the same AV_3Sb_5 structural family, the V-I curves after zero-field cooling and after field-training sweeps from ± 9 T to zero are nearly identical, as shown in Fig. 4a. Thus the critical-current memory is not a generic consequence of exfoliation, hBN encapsulation, contact geometry, or kagome-band normal-state physics. In thin-flake $NbSe_2$, a well-studied layered superconductor, zero-field-cooled and field-trained curves also overlap, as shown in Fig. 4b. If trapped flux in the measurement circuit or contact heating were the dominant cause, comparable memory would be expected in at least one of these control devices. The selective appearance in RbV_3Sb_5 instead points to an intrinsic superconducting property. Additionally, control measurements on CsV_3Sb_5 and $NbSe_2$ at 1.8 K also show no critical-current memory (Fig. S2 in Supplementary Information).

Symmetry constraint.—The central experimental observation is the combination of in-plane-field magnetotransport, sweep-direction-dependent critical current, and material selectivity. Microscopic reversibility implies the following nonlinear transport constraint when all time-reversal-odd internal variables are reversed together with current and magnetic field [30–32]:

$$V_\eta(I,\mathbf{B}) = V_{\bar{\eta}}(-I,-\mathbf{B}), \qquad I^+_{c,\eta}(\mathbf{B}) = I^-_{c,\bar{\eta}}(-\mathbf{B}). \quad (1)$$

Here η labels the internal superconducting configuration, $\bar{\eta}$ is its time-reversed partner, and I_c^+ and I_c^- denote the positive and negative switching-current magnitudes. If no trainable time-odd superconducting variable is present, $\eta = \bar{\eta}$ and Eq. (1) reduces to the usual even-field constraint on the critical-current envelope, after the current polarity is also reversed. The important point is not merely that the forward and backward sweeps differ. In a single uninterrupted backward sweep from $+0.5$ T to -0.3 T, the critical current measured at $+B$ is not the same as that measured at $-B$ on the same branch: the maximum occurs near $+0.2$ T, whereas the corresponding negative-field side is lower. Equivalently, for the branch selected by the backward sweep one observes [21, 22, 30–32]

$$I_{c,\leftarrow}(+|B|) \neq I_{c,\leftarrow}(-|B|), \quad (2)$$

and the forward sweep gives the mirror-related inequality with the opposite preferred sign. This single-branch asymmetry explicitly violates the time-reversal expectation for a superconducting state with no internal moment. It therefore requires a superconducting variable that is odd under time reversal and that remains metastably trained while the external field is swept.

A natural minimal candidate is an in-plane spin polarization of Cooper pairs. In the standard theory of spin-triplet superconductivity, the gauge-invariant spin polarization of a nonunitary condensate is proportional

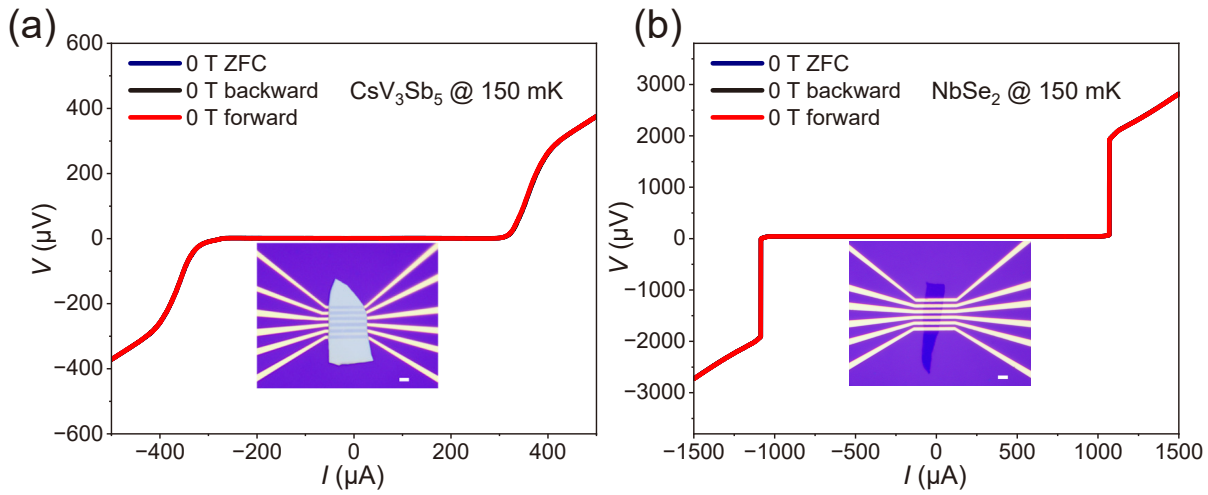


FIG. 4. **Control experiments.** (a) Field-training test on CsV_3Sb_5 at 150 mK. The blue curve is the zero-field-cooled trace; the black and red traces are obtained after in-plane training sweeps from +9 T and −9 T back to zero, respectively. No appreciable critical-current hysteresis is observed. (b) Corresponding test on thin-flake $NbSe_2$ at 150 mK. Because $NbSe_2$ is an Ising superconductor, the training field is applied out of plane. The zero-field-cooled and field-trained curves overlap. Insets show optical images of the devices; scale bars are 3 μm.

to [22, 33, 34]

$$\mathbf{S}_{\rm pair}(\mathbf{k}) = \frac{\mathrm{i}}{2}\,\mathbf{d}(\mathbf{k}) \times \mathbf{d}^*(\mathbf{k}). \tag{3}$$

We use Eq. (3) only as a symmetry diagnostic: it shows how a superconducting condensate can carry a trainable moment without specifying a unique microscopic $\mathbf{d}(\mathbf{k})$. This restraint is important. The present transport data support an in-plane superconducting moment, but they do not alone determine a particular D_{2h} irreducible representation, nodal topology, or edge-state spectrum.

The field dependence of such a moment can be captured by a domain free energy. For domains labeled by $\sigma = \pm 1$, corresponding to opposite in-plane superconducting moments, the leading terms are [21, 22, 33, 34]

$$\begin{aligned} F_\sigma(B,s) &= F_0 + \epsilon_{\rm DW} n_{\rm DW}(s) - \sigma M_0 B, \\ F_+ - F_- &= -2M_0 B. \end{aligned} \tag{4}$$

Here M_0 is the magnitude of the in-plane superconducting moment, $n_{\rm DW}$ is the density of domain walls relevant to the current path, $\epsilon_{\rm DW}$ is the domain-wall energy scale, and s labels the field history. Equation (4) explains the sign reversal of the I_c maximum: a negative field favors one domain orientation, a positive field favors the opposite orientation, and after field reversal the system can remain in a metastable mixed-domain texture.

Why $I_c^{\rm ZFC}(0)$ is larger than any field-trained I_c.—The inequality $I_c^{\rm ZFC}(0) > I_{c,\rm max}^{\rm FT}$ is not a contradiction of the domain interpretation. It says that the field-trained state is locally biased but globally less capable of carrying a dissipationless current. A minimal expansion of the critical current around the zero-field-cooled state combines three effects: quadratic finite-field pair breaking, a linear coupling to the trained moment, and suppression by domain-wall weak links. To lowest order one may write [21, 22, 35, 36]

$$\frac{I_c(B,s)}{I_c^{\rm ZFC}(0)} \simeq 1 - \alpha_{\rm pb} B^2 + \alpha_m m_s B - \lambda n_{\rm DW}(B,s), \tag{5}$$

where $m_s = \pm 1$ is the trained moment direction set by the sweep history. The term $\alpha_{\rm pb}B^2$ represents the usual even-in-field depairing of a superconducting condensate. The term $\alpha_m m_s B$ is allowed because the trained state itself breaks time reversal. The last term describes the reduction of the percolating critical current by domain walls or Josephson-like weak links.

The branch maximum follows from the full expression. Differentiating Eq. (5) gives the peak condition [21, 22, 35, 36]

$$2\alpha_{\rm pb} B_{\rm pk} = \alpha_m m_s - \lambda\, \partial_B n_{\rm DW}(B_{\rm pk}, s), \tag{6}$$

and the corresponding field-trained peak current is [21, 22, 35, 36]

$$\frac{I_{c,\rm max}^{\rm FT}}{I_c^{\rm ZFC}(0)} \simeq 1 - \alpha_{\rm pb} B_{\rm pk}^2 + \alpha_m m_s B_{\rm pk} - \lambda n_{\rm DW}(B_{\rm pk}, s). \tag{7}$$

Equations (6) and (7) separate the two roles of the field. If the domain-wall density changes slowly near the peak, the derivative term in Eq. (6) only weakly renormalizes the position, so $B_{\rm pk} \approx B_0 \equiv \alpha_m m_s/(2\alpha_{\rm pb})$. The linear coupling then shifts the maximum to opposite signs for opposite sweep directions, as observed in Figs. 2 and 3. However, the ZFC state is measured

at $B = 0$, where finite-field depairing is absent, and it is not forced through a high-field training cycle that can trap metastable domain walls. Within the same phenomenological depairing and weak-link description, the slowly varying limit gives a field-trained maximum smaller than the ZFC value whenever $\lambda n_{\mathrm{DW}}(B_0, s) > \alpha_m^2/(4\alpha_{\mathrm{pb}})$ [21, 22, 35, 36].

This condition is physically reasonable for a current-biased thin flake. The critical current is controlled by the weakest link along the percolating superconducting path, not by the average local condensation energy. Field training can align the moment of some domains and lower their local Zeeman energy, while the same process generates domain boundaries between regions with different polarization histories. Those boundaries are natural sites for phase slips, reduced order-parameter amplitude, or Josephson-like current bottlenecks. Thus a finite field can reveal and train the internal superconducting moment without increasing the global current above the equilibrium zero-field-cooled value. The observed ratio $I_{c,\mathrm{max}}^{\mathrm{FT}}/I_c^{\mathrm{ZFC}}(0) \approx 25/35$ indicates that the weak-link and finite-field penalties are substantial.

This interpretation also separates the present effect from normal-state loop-current order. Loop-current proposals for the charge-density-wave state generally produce orbital moments with a dominant out-of-plane character [16–19, 21]. The critical-current memory reported here is driven by an in-plane magnetic field, occurs only in the superconducting switching behavior, and is absent in CsV_3Sb_5 despite the closely related kagome structure. The most economical explanation is therefore a superconducting, rather than purely normal-state, internal moment in RbV_3Sb_5.

Outlook and conclusion.—The present work establishes a transport constraint that future microscopic theories should satisfy. For example, future theories should explain why RbV_3Sb_5 supports a trainable in-plane superconducting moment, why CsV_3Sb_5 does not show comparable critical-current memory under the same type of test. Phase-sensitive Josephson interferometry, scanning probes of domain textures, Kerr or μSR measurements under calibrated in-plane fields, and tunneling spectroscopy on the same type of thin flakes would be especially valuable.

In summary, thin-flake RbV_3Sb_5 exhibits critical-current hysteresis under in-plane magnetic fields. The maximum switching current is displaced from zero field in a sweep-direction-dependent manner, but the largest current overall occurs after zero-field cooling. Control experiments on CsV_3Sb_5 and $NbSe_2$ do not show the effect. A minimal model of spin-polarized superconducting domains possibly explains all of these observations: the field trains an in-plane superconducting moment, field reversal creates metastable domain coexistence, and domain walls suppress the percolating supercurrent. Our findings therefore provide an experimental signature of unconventional superconductivity in kagome RbV_3Sb_5 and also make the kagome RbV_3Sb_5 distinct from CsV_3Sb_5.

This work was supported by the National Key Research and Development Program of China (No. 2022YFA1403700), the Guangdong Basic and Applied Basic Research Foundation (No. 2022B1515130005), and Guangdong Province 2020KCXTD001.

* These authors contributed equally.
† linbenchuan@iqasz.cn
‡ wangshuo@iqasz.cn

[1] Ortiz B R, Gomes L C, Morey J R, Winiarski M, Bordelon M, Mangum J S, Oswald I W H, Rodriguez-Rivera J A, Neilson J R, Wilson S D, Ertekin E, McQueen T M and Toberer E S 2019 *Phys. Rev. Materials* **3** 094407
[2] Ortiz B R, Teicher S M L, Hu Y, Zuo J L, Sarte P M, Schueller E C, Abeykoon A M M, Krogstad M J, Rosenkranz S, Osborn R, Seshadri R, Balents L, He J and Wilson S D 2020 *Phys. Rev. Lett.* **125** 247002
[3] Yin J X, Lian B and Hasan M Z 2022 *Nature* **612** 647–657
[4] Jiang K, Wu T, Yin J X, Wang Z, Hasan M Z, Wilson S D, Chen X and Hu J 2023 *Natl. Sci. Rev.* **10** nwac199
[5] Wang Y, Wu H, McCandless G T, Chan J Y and Ali M N 2023 *Nat. Rev. Phys.* **5** 635–658
[6] Chen H, Yang H, Hu B *et al.* 2021 *Nature* **599** 222–228
[7] Nie L, Sun K, Ma W *et al.* 2022 *Nature* **604** 59–64
[8] Deng H, Qin H, Liu G *et al.* 2024 *Nature* **632** 775–781
[9] Yan X Y, Deng H, Yang T, Liu G, Song W, Miao H, Tu Z, Lei H, Wang S, Lin B C, Qin H and Yin J X 2024 *Chinese Phys. Lett.* **41** 097401
[10] Duan W, Nie Z, Luo S, Yu F, Ortiz B R, Yin L, Su H, Du F, Wang A, Chen Y, Lu X, Ying J, Wilson S D, Chen X, Song Y and Yuan H 2021 *Sci. China Phys. Mech. Astron.* **64** 107462
[11] Xu H S, Yan Y J, Yin R, Xia W, Fang S, Chen Z, Li Y, Yang W, Guo Y and Feng D L 2021 *Phys. Rev. Lett.* **127** 187004
[12] Roppongi M, Ishihara K, Tanaka Y, Ogawa K, Okada K, Liu S, Mukasa K, Mizukami Y, Uwatoko Y, Grasset R, Konczykowski M, Ortiz B R, Wilson S D, Hashimoto K and Shibauchi T 2023 *Nat. Commun.* **14** 667
[13] Zhong Y, Liu J, Wu X *et al.* 2023 *Nature* **617** 488–492
[14] Guguchia Z, Mielke III C, Das D *et al.* 2023 *Nat. Commun.* **14** 153
[15] Gu Y, Zhang Y, Feng X, Jiang K and Hu J 2022 *Phys. Rev. B* **105** L100502
[16] Jiang Y X, Yin J X, Denner M M *et al.* 2021 *Nat. Mater.* **20** 1353–1357
[17] Mielke III C, Das D, Yin J X, Liu H, Gupta R, Jiang Y X, Medarde M, Wu X, Lei H C, Chang J, Dai P, Si Q, Miao H, Thomale R, Neupert T, Shi Y, Khasanov R, Hasan M Z, Luetkens H and Guguchia Z 2022 *Nature* **602** 245–250
[18] Khasanov R, Das D, Gupta R, Mielke III C, Elender M, Yin Q, Tu Z, Gong C, Lei H, Ritz E T, Fernandes R M, Birol T, Guguchia Z and Luetkens H 2022 *Phys. Rev. Research* **4** 023244

[19] Feng X, Jiang K, Wang Z and Hu J 2021 *Sci. Bull.* **66** 1384–1388
[20] Xu Y, Ni Z, Liu Y, Ortiz B R, Deng Q, Wilson S D, Yan B, Balents L and Wu L 2022 *Nat. Phys.* **18** 1470–1475
[21] Wang S, Feng X, Fang J Z, Peng J P, Sun Z T, Yang J J, Xiong L, Liu J, Zhao J J, Kang N, Wu X S, Zhang Z, Fu X, Law K T, Lin B C and Yu D 2026 *Nat. Commun.* **17** 1310
[22] Feng X, Sun Z T, Lin B C and Law K T 2025 *arXiv:2501.10998 [cond-mat.supr-con]*
[23] Ginzburg V L 1958 *Sov. Phys. JETP* **34** 1
[24] Caswell H L 1965 *J. Appl. Phys.* **36** 80–84
[25] Dew-Hughes D 2001 *Low Temp. Phys.* **27** 713–722
[26] Ji L, Rzchowski M S, Anand N and Tinkham M 1993 *Phys. Rev. B* **47** 470–483
[27] Semenov S V and Balaev D A 2019 *J. Supercond. Nov. Magn.* **32** 2409–2419
[28] Semenov S V, Balaev D A and Petrov M I 2021 *Phys. Solid State* **63** 1069–1080
[29] Muné P, Fonseca F C, Muccillo R and Jardim R F 2003 *Physica C* **390** 363–373
[30] Onsager L 1931 *Phys. Rev.* **37** 405–426
[31] Casimir H B G 1945 *Rev. Mod. Phys.* **17** 343–350
[32] Chen C Z, He J J, Ali M N, Lee G H, Fong K C and Law K T 2018 *Phys. Rev. B* **98** 075430
[33] Leggett A J 1975 *Rev. Mod. Phys.* **47** 331–414
[34] Sigrist M and Ueda K 1991 *Rev. Mod. Phys.* **63** 239–311
[35] Tinkham M 2004 *Introduction to Superconductivity* 2nd ed (New York: Dover)
[36] Likharev K K 1979 *Rev. Mod. Phys.* **51** 101–159